Coatings **2013**, *3*, 16-25; doi:10.3390/coatings3010016

OPEN ACCESS

coatings

ISSN 2079-6412

www.mdpi.com/journal/coatings/

Article

Polyurethane Coatings Reinforced by Halloysite Nanotubes

Xin Li, Irina Nikiforow, Katja Pohl, Jörg Adams and Diethelm Johannsmann *

Institute of Physical Chemistry, Clausthal University of Technology, 38678 Clausthal-Zellerfeld, Germany; E-Mails: x.li@tu-clausthal.de (X.L.); irina.nikiforow@tu-clausthal.de (I.N.); kpoh@tu-clausthal.de (K.P.); pcja@tu-clausthal.de (J.A.)

* Author to whom correspondence should be addressed; E-Mail: johannsmann@pc.tu-clausthal.de; Tel.: +49-(0)-5323-72-3768; Fax: +49-(0)-5323-72-4835.

Received: 18 December 2012; in revised form: 10 January 2013 / Accepted: 15 January 2013 / Published: 18 January 2013

Abstract: The pencil hardness of a two-component polyurethane coating was improved by adding halloysite nanotubes to the recipe at a weight fraction of less than 10%. The pencil hardness was around F for the unfilled coating and increased to around 2H upon filling. It was important to silanize the surface of the filler in order to achieve good coupling to the matrix. Sonicating the sample during drying also improved the hardness. Scanning electron micrographs suggest that the nanotubes are always well immersed into the bulk of the film. With a thickness between 10 and 20 µm, the optical clarity was good enough to clearly read letters through the film. The films can be used in applications where transparency is required.

Keywords: polyurethane coatings; halloysite nanotubes; scratch resistance

---

1. Introduction

Fiber reinforced plastics have been highly successful as light-weight structural materials with good stiffness, strength and durability [1]. Their superior properties go back to the material's composite nature. Roughly speaking, the fiber imparts stiffness to the structure and redistributes localized stress, while the matrix provides for cohesion and dissipates energy resulting from sudden impacts. Stiffness, strength and durability are also essential performance parameters for protective coatings [2,3]. Given that fibers improve the properties of structural materials, one may attempt to apply similar concepts to coatings. Filling coatings with inorganic particles is a well-known strategy to improve scratch resistance [4–8]. A good adhesion between the matrix and the filler is critical, which is often achieved

by silanization [9,10]. Presently, most inorganic fillers are either close to spherical or composed of small platelets [11]. In order to achieve a significant improvement in scratch resistance, nanoparticles are usually added at a weight fraction in the range of 20% or more [12–15]. While the mechanism by which nanoparticles improve hardness is under debate, it is clear that nanoparticles must make up a significant fraction of the overall volume in order to be mechanically active. At least in principle, one can hope to improve the mechanical properties of a coating with smaller levels of loading when employing fibers. Due to their elongation, fibers more easily form mechanically coupled networks than spheres. For the sake of processing, one has to employ "short fibers", that is, fibers, which do not prevent a flow of the material [16]. These will be distributed more or less randomly inside the coating, and some orientational order may result from the flow during application of the film. A "short" fiber implies a fiber length much below the film thickness, which rules out the fibers normally employed for structural materials. "Nanofibers" have to be employed. Fiber reinforcement on the nanoscale has been thoroughly studied using carbon nanotubes (CNTs) [17,18]. The success is mixed [19], where major problems are control of the morphology and adhesion between the fiber and the matrix [20].

In the work reported below, we have investigated to what extent halloysite nanotubes (HNTs) can improve the scratch resistance of coatings formed from a commercial two-component polyurethane formulation. HNTs are phyllosilicates with a tubular shape [21]. Chemically, halloysite is similar to kaolinite, however the difference is that there is a thin layer of water between successive layers. This layer relaxes the requirement of positional registry between the layers and thereby allows for bending. The curvature occurs towards the side with the alumina surface. The outside and the inside of the tube, therefore, are a silica surface and an alumina surface, respectively. Typical lengths of the fibers employed here are between 1 and 3 μm. The outer diameter is around 50 nm. These geometrical parameters (taken from [22]) were confirmed by scanning electron microscopy in our previous work [23]. The refractive index of halloysite is $n \sim 1.54$. Given that n is not particularly high, (polyurethanes have $n \sim 1.5$), one expects HNTs to scatter light only moderately. The density of HNTs is the density typical of silica, which is around 2.53 g/cm³. Combined with the size as quoted above, this density implies the HNTs sediment in water unless they are stabilized by a flocculating agent. Since HNTs are a natural product, they can be relatively cheap. In this particular case, the supplier charged €100 for 500 g. The safety data sheet does not categorize the HNTs as hazardous.

A recent review on various applications of HNTs is provided in [24]. These authors elaborate at length on the fact that HNTs are hollow and, therefore, may function as nanocontainers in the context of corrosion prevention [25], selective catalysis [26], self-healing [27] and drug delivery [28]. The fact that HNTs are hollow is not important for our work. HNTs are simply used for the purpose of structural reinforcement. The use of HNTs as a filler for polymers, has, for instance, been reported by Rooj *et al.* [29]. These authors have reinforced a rubber. Interestingly, the inorganic filler not only increased the mechanical modulus, but the decomposition temperature, as well. As with all fillers designed for structural reinforcement, good adhesion is required between the matrix and the filler. For this purpose, silica surfaces are often silanized. Silanization and other means of surface functionalization of HNTs are, for instance, reported in references [30] and [31], and we followed reference [31].

As the results show, there is a clear improvement in pencil hardness even at HNT weight fractions below 10%. We compare these results to the hardening obtained with silica spheres. The spheres also improved the hardness, but the dependence on the added amount was more gradual.

2. Materials

For the matrix, we used a commercial waterborne two component (2K) polyurethane. The polyol component and the isocyanate component were Bayhydrol® A XP 2695 and Desmodur® N 3900, respectively (kindly provided by Bayer MaterialScience). Bayhydrol® A XP 2695 is delivered as an emulsion with a polymer content of 41 wt%. It has a viscosity of 2500 mPa s (at 23 °C) and a pH of 7.7. The hydroxyl content is 5% [32]. Desmodur® N 3900 is a polyisocyanate resin based on hexamethylene diisocyanate (HDI); it is delivered in pure form. The viscosity at 23 °C is 730 mPa s; the isocyanate content is 23.5 wt% [33]. HNTs were purchased in powder form from Sigma-Aldrich. Surface functionalization of the HNTs with (3-aminopropyl)-triethoxysilane (APTES) occurred as described in [31]. APTES was obtained from Sigma-Aldrich; dry toluene was obtained from Acros Organics. Silica nanoparticles, (NexSil™ 85NH4) were provided by Nordmann, Rassmann GmbH. These particles carry a negative charge. The diameter is 85 nm. NexSil™ 85NH4 is supplied as an aqueous dispersion with a solids content of 40 wt%.

3. Film Preparation

In a first step, the HNTs (as received or silanized) were dispersed in water by stirring for 10 min. The amount of water was always chosen such that the solids content of the dispersion obtained after addition of the polyol and the isocyanate was between 43 wt% and 45 wt%. Only in this range of solids content was film formation successful. In a second step, the polyol (10 g Bayhydrol® A XP 2695, an aqueous dispersion) was added and the mixture was again stirred for 10 min. Importantly, the high viscosity now prevents sedimentation of the HNTs. The high viscosity is critical to a successful processing. (In water, HNTs sediment after one stops agitating the dispersion.) Isocyanate (4.32 g Desmodur® N 3900) was added in the last step. The NCO to OH ratio was fixed at 2:1, as recommended by the supplier. The final mixture was stirred for another 10 min and sonicated for 4 min (Branson Sonifier 450 with 70% output). For the samples containing silica spheres, the protocol was reversed. Silica spheres were added in the last step (that is, after addition of the isocyanate).

Application of the dispersion to microscope slides occurred by casting from dispersion. After the material had been applied, the substrate was held vertically, thereby allowing excess material to flow off. The dry film thickness as determined gravimetrically was between 10 and 20 µm. Once the coating had solidified to the extent that it would not flow under gravity, the samples were transferred to an oven and cured at 60 °C over night. Some samples were subjected to ultrasound before curing. For sonication, the samples were placed in a petri dish, which was placed into an ultrasonic bath (Bandelin Sonorex RK 106). Note: the samples stayed dry; the Petri dish floated on the water surface. Ultrasound was applied for 15 min. No measures were undertaken to optimize film formation [34]. The surfaces of the films formed from the filled PU showed defects (mostly of the orange skin type; see left-hand-side in Figure 2), the removal of which was outside the scope of this work.

For the quantification of HNT content, we use both weight fraction (wt%) and volume fraction (vol%). Assuming a density of polyurethane of 1.05 g/cm³ and an average density of the HNTs of 2.53 g/cm³, we arrive at the converted values provided in Table 1.

Table 1. Halloysite nanotubes (HNT) fractions in wt% and vol%.

Fraction of HNTs in wt%	Fraction of HNTs in vol%
0.5	0.2
1	0.4
2	0.8
3	1.3
4	1.7
5	2.1
10	4.4
20	9.4
30	15.1

The volume fraction is needed to discuss the percolation threshold in Section 5.

4. Characterization

Silanization of the HNT surface was checked by *FTIR Spectroscopy* (Spectrum BX FT-IR, PerkinElmer Inc.). Specimens were prepared by pelleting 1 mg of the HNTs with 100 mg of KBr. Spectra of the pure and the silanized HNTs are shown in Figure 1. Table 2 shows the band assignment. Dashed circles in the figure indicate lines originating from APTES. The bands at 2930 cm^{-1} and 1400 cm^{-1} belong to the symmetric stretching mode and the deformation mode of the CH_2 groups [35].

Table 2. Band assignments for the Fourier transform infrared (FTIR) spectra shown in Figure 1 [31]. Bold: Bands originating from silanization.

Wave number [cm^{-1}]	Mode of vibration
3600–3700	O–H stretching, inner hydroxyl groups
3400–3500	O–H stretching, H_2O
2900–3000	**C–H stretching, CH_2**
1630	O–H deformation, H_2O
1490, 1380	**C–H deformation, CH_2**
1020, 1080	Si–O stretching
900	O–H deformation, inner hydroxyl groups
790, 750, 700	Si–O stretching
530	Al–O–Si deformation
470	Si–O–Si deformation
430	Si–O deformation

Scratch resistance was quantified by measurements of the *Pencil Hardness*. The pencil hardness scale extends from 9H (hard) to 9B (not hard). We followed ISO 15184, using a Wolf-Wilburn Pencil Hardness tester (BYK-Gardner, Geretsried, Germany).

The surface morphology of the films was investigated by means of *Field Emission Scanning Electron Microscopy* (FESEM). The instrument employed was the unit Helios Nanolab 600, supplied by FEI (Eindhoven). The vCD detector (low voltage, high contrast backscatter electron detector) was used. The samples were coated with a thin carbon layer to improve conductivity. The voltage and the current were 5.0 kV and 43 pA, respectively.

Figure 1. FTIR spectra of pure HNTs (thin black line) and APTES functionalized HNTs (thick red line, color online). Dashed circles indicate bands originating from silanization. The absorption bands at 1400 cm^{-1} and 2900 cm^{-1} are the vibrations of the methylene group.

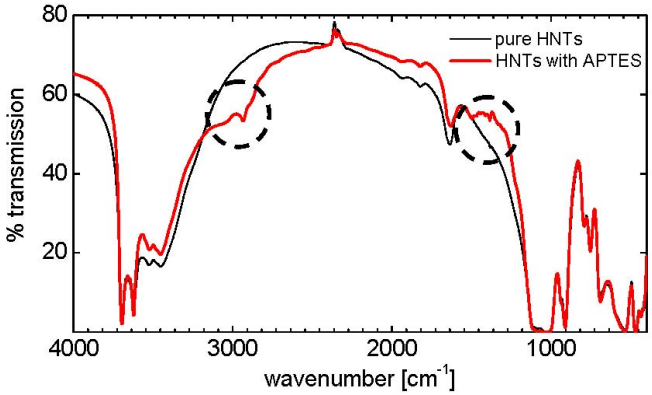

5. Results and Discussion

5.1. Optical Appearance

With HNTs (silanized or not) added at a fraction less than or equal to 10 wt%, the appearance of the films to the naked eye was unchanged. Figure 2 compares an HNT-filled film (unsilanized tubes) to a film filled with NexSil silica spheres. Clearly, the HNT-filled film allows one to read the text underneath. The degradation in transparency is mostly due to an orange skin, which has developed at the film surface. When making the comparison, one has to be aware of the fact that the particle diameter was 85 nm for the silica spheres. Silica spheres of that size are known to scatter light rather efficiently. The purpose of the figure is to show that the films filled with HNTs are still transparent, even though the length of the rods exceeds the wavelength of light, λ. As is well-known, equally transparent coatings can be produced with silica nanospheres, provided that sufficiently small spheres are employed.

5.2. Scanning Electron Microscopy

Figure 3 shows scanning electron micrographs of an HNT-filled film produced by casting (A), an HNT-filled film produced by casting and subsequent treatment with ultrasound (B) and a film from previous work, which contained 80 wt% of Halloysite in an acrylic matrix (C) [23]. The latter image serves for comparison. The HNTs were not silanized. Images taken on films containing silanized HNTs (not shown) look similar to what is seen in panels A and B. These images suggest that the nanotubes were all well immersed in the film. Panel C has been added to show what HNTs sticking out of the film surface would have looked like. Well immersed nanotubes were found, regardless of whether or not the sample had been sonicated. Clearly, the width of the features shown in panels A and B exceeds the diameter of the nanotubes themselves. This may happen because what is imaged is not the tube itself, but rather a slight nonuniformity of the PU surface covering the tube. Another possibility is bundling. Importantly, the sample shown in panel C (which has HNTs exposed at the surface) had poor scratch resistance (<9B). This makes sense, because nanotubes sticking out will presumably transport stress from the surface to the bulk and produce localized damage. HNTs sticking out of the surface will increase the friction, thereby promoting damage. The working hypothesis had

been that sonication would help to generate a flat film-air interface, entirely composed of PU. As the images show, sonication is not actually needed to achieve this situation.

Figure 2. Photographs taken through a sample containing 10 wt% HNTs (**left**) and a sample containing 10 wt% silica spheres with a diameter of 85 nm (**right**). Both films are 16 μm thick. Clearly, the film containing HNTs still is moderately transparent.

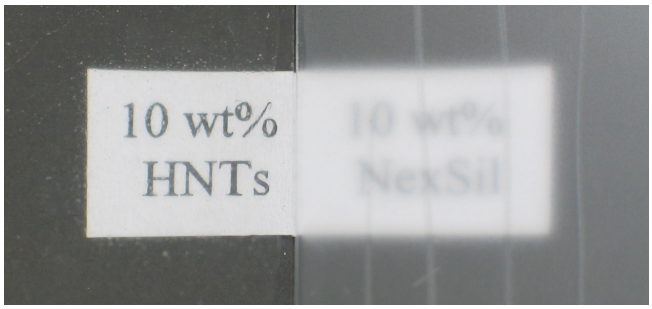

Figure 3. Scanning electron micrographs of films filled with unsilanized HNTs (10 wt%). (**A**) Cast; (**B**) Cast with subsequent ultrasound treatment; (**C**) Sample containing 80 wt% HNTs in an acrylic matrix. Panels A and B suggest that the HNTs are immersed into the bulk of the film. Panel C shows a counter example, where the tubes stick out of the surface. All scale bars correspond to 5 μm. Panel C is reprinted with permission from reference [23] (Copyright 2012, American Chemical Society).

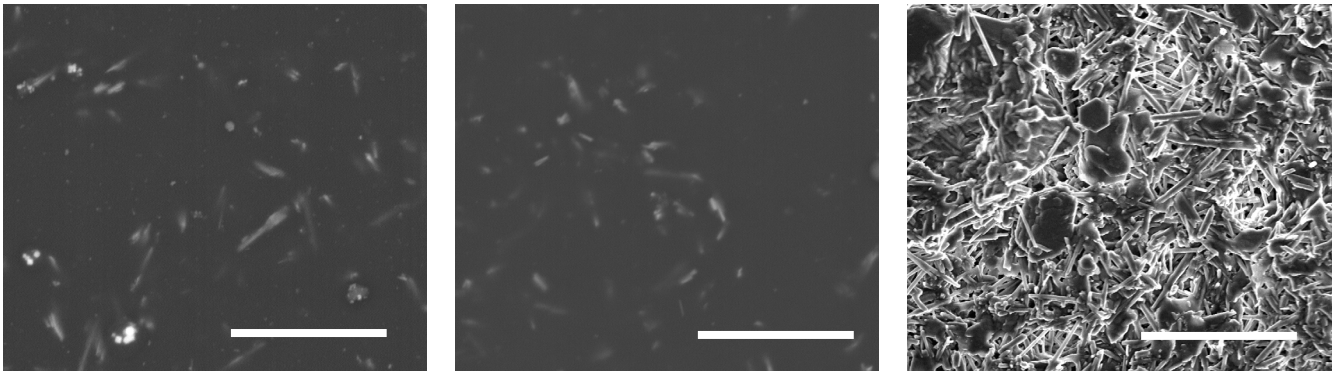

(**A**) (**B**) (**C**)

5.3. Pencil Hardness

Figure 4 summarizes the essential outcome of this study. An improvement of scratch resistance by about two units is achieved by adding as little as 5 wt% silanized HNTs. (The figure shows an improvement of three units, but there is an uncertainty of one unit). 5 wt% of HNTs correspond to about 2 vol%. These samples had not been treated with ultrasound. Untreated fibers (circles in Figure 4) only induce a moderate improvement, and they only do so at a weight fraction of 30%. Silica spheres (triangles in Figure 4) also improve the pencil hardness, but the effect is more gradual than with Halloysite tubes. For silanized nanotubes, there is a clear threshold at around 5 wt%. We interpret this threshold as the critical density needed to establish a mechanical network inside the film.

The percolation threshold of 5 wt% (corresponding to about 2.1 vol%, *cf.* Table 1) should be discussed in the frame of percolation theory as, for instance, put forward by Foygel *et al.* in [36].

Using a Monte Carlo simulation, these authors calculated the critical fractional volume (CFV) for percolation as a function of the aspect ratio of tubes, *a*. In the limit of high aspect ratio, they arrive at the estimate of CFV ~ 0.60/*a*. Inserting an aspect ratio of about 60 (diameter ~ 50 nm, length ~ 3 µm), this translates to a threshold of 1 vol%. Clearly, our experimental result differs by a factor of 2. Reasons might be a broad distribution of fiber lengths, fiber bundling, incomplete dispersion of the fibers or the fact that the improvement of scratch resistance occurs at a volume fraction somewhere above the percolation threshold. Indications of bundling are actually seen in Figure 3(A,B). The width of elongated shapes exceeds the width of the nanotubes. This may have to do with the imaging process, but it may also be caused by bundling.

Figure 5 separately addresses the issue of sonication. It compares the pencil hardness achieved with non-silanized HNTs with and without sonication. The open circles are the same data as in Figure 4. The squares are pencil hardness obtained with the same material, but it was floated on an ultrasonic bath while drying. As the figure shows, an improvement is found for these process conditions. The improvement achieved with functionalization and the improvement achieved with sonication both amount to about two units. There were no synergetic effects: silanized nanotubes treated with ultrasound achieved about the same pencil hardness as the silanized HNTs with no ultrasound treatment. We have at this point not systematically investigated the dependence of pencil hardness on duration of the ultrasound treatment. Figure 5 demonstrates that an ultrasound treatment has potential for improvement. The details need further studies.

Figure 4. Pencil hardness *versus* degree of loading for non-silanized HNTs (circles), silanized HNTs (squares) and silica spheres (triangles).

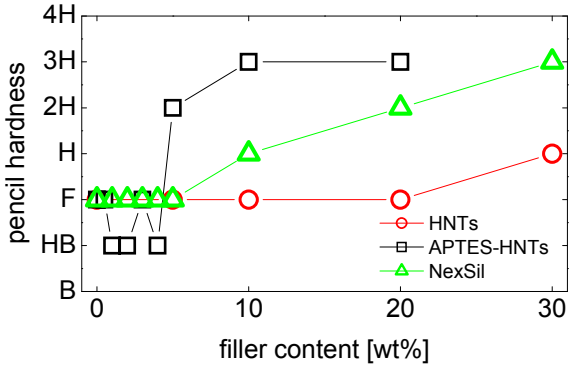

At this point, it must also be remembered that a pencil hardness of 2H does not constitute a spectacular result. Much harder films exist. The improvement achieved here started from a reference material, the hardness of which was moderate (B). Whether or not a similar improvement can be achieved for materials that already have a good hardness in the unfilled state was not tested. The emphasis here is on the fact that an improvement in hardness was achieved with low degrees of loading, while maintaining optical transparency. Potential applications presumably will be in areas, where scratch resistance *per se* is not the only engineering target and the amount of filler needs to be maintained low. Such layers could, for instance, be adhesives [19] or anti-fog coatings [37].

Figure 5. Pencil hardness *versus* degree of loading for non-silanized HNTs with (squares) and without (circles) sonication of the sample during drying.

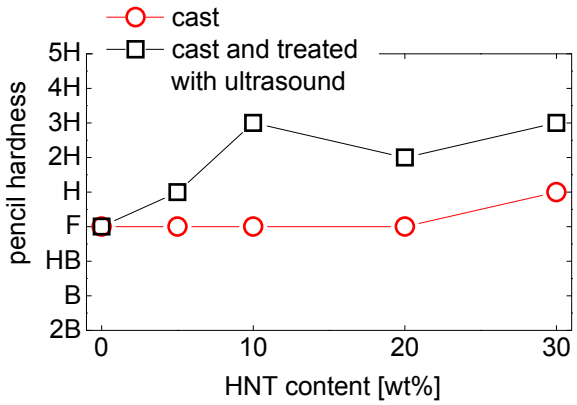

6. Conclusions

An improvement in pencil hardness (where pencil hardness was chosen as the indicator of scratch resistance) has been achieved by adding Halloysite nanotubes to a polyurethane formulation at a level as low as 5 wt%. This finding can be rationalized by HNTs forming a mechanical network inside the polymer matrix due to their elongated shape. SEM micrographs showed that the nanotubes were all well immersed in the bulk of the film. The films were optically transparent. Applications will most likely be in areas where hardness needs to be achieved in combination with other, possibly conflicting, engineering targets.

Acknowledgements

We thank André Blasig from the Institute of Non-Metallic Materials at Clausthal University of Technology for taking the FESEM images. This work was funded by the Deutsche Forschungsgemeinschaft (DFG, Grant No. Jo 278/18-1).

References

1. Tong, L.; Mouritz, A.P.; Bannister, S.O. *3D Fibre Reinforced Polymer Composites*, 1st ed.; Elsevier Science & Technology: Amsterdam, The Netherlands, 2002.
2. Gerhart, H.L. Protective Coatings. *Ind. Eng. Chem.* **1965**, *57*, 52–60.
3. Seubert, C.; Nietering, K.; Nichols, M.; Wykoff, R.; Bollin, S. An Overview of the Scratch Resistance of Automotive Coatings: Exterior Clearcoats and Polycarbonate Hardcoats. *Coatings* **2012**, *2*, 221–234.
4. Zhou, S.X.; Wu, L.M.; Sun, J.; Shen, W.D. The change of the properties of acrylic-based polyurethane via addition of nano-silica. *Progr. Org. Coating* **2002**, *45*, 33–42.
5. Dasari, A.; Yu, Z.Z.; Mai, Y.W. Fundamental aspects and recent progress on wear/scratch damage in polymer nanocomposites. *Mater. Sci. Eng. R Rep.* **2009**, *63*, 31–80.
6. Friedrich, K.; Zhang, Z.; Schlarb, A.K. Effects of various fillers on the sliding wear of polymer composites. *Compos. Sci. Tech.* **2005**, *65*, 2329–2343.

7. Mills, D.J.; Jamali, S.S.; Paprocka, K. Investigation into the effect of nano-silica on the protective properties of polyurethane coatings. *Surf. Coating Tech.* **2012**, *209*, 137–142.
8. Sangermano, M.; Messori, M. Scratch Resistance Enhancement of Polymer Coatings. *Macromol. Mater. Eng.* **2010**, *295*, 603–612.
9. Howarter, J.A.; Youngblood, J.P. Optimization of silica silanization by 3-aminopropyltriethoxysilane. *Langmuir* **2006**, *22*, 11142–11147.
10. Mora-Barrantes, I.; Rodriguez, A.; Ibarra, L.; Gonzalez, L.; Valentin, J.L. Overcoming the disadvantages of fumed silica as filler in elastomer composites. *J. Mater. Chem.* **2011**, *21*, 7381–7392.
11. Jordan, J.; Jacob, K.I.; Tannenbaum, R.; Sharaf, M.A.; Jasiuk, I. Experimental trends in polymer nanocomposites—A review. *Mater. Sci. Eng. A* **2005**, *393*, 1–11.
12. Glasel, H.J.; Bauer, F.; Ernst, H.; Findeisen, M.; Hartmann, E.; Langguth, H.; Mehnert, R.; Schubert, R. Preparation of scratch and abrasion resistant polymeric nanocomposites by monomer grafting onto nanoparticles, 2—Characterization of radiation-cured polymeric nanocomposites. *Macromol. Chem. Phys.* **2000**, *201*, 2765–2770.
13. Barna, E.; Bommer, B.; Kursteiner, J.; Vital, A.; von Trzebiatowski, O.; Koch, W.; Schmid, B.; Graule, T. Innovative, scratch proof nanocomposites for clear coatings. *Compos. Appl. Sci. Manuf.* **2005**, *36*, 473–480.
14. Bauer, F.; Ernst, H.; Hirsch, D.; Naumov, S.; Pelzing, M.; Sauerland, V.; Mehnert, R. Preparation of scratch and abrasion resistant polymeric nanocomposites by monomer grafting onto nanoparticles, 5(a)—Application of mass Spectroscopy and atomic force microscopy to the characterization of silane-modified silica surface. *Macromol. Chem. Phys.* **2004**, *205*, 1587–1593.
15. Amerio, E.; Sangermano, M.; Colucci, G.; Malucelli, G.; Messori, M.; Taurino, R.; Fabbri, P. UV curing of organic-inorganic hybrid coatings containing polyhedral oligomeric silsesquioxane blocks. *Macromol. Mater. Eng.* **2008**, *293*, 700–707.
16. Jones, R.F. *Guide to Short Fiber Reinforced Plastics*, 1st ed.; Hanser Publishers: Munich, Germany, 1998.
17. Breuer, O.; Sundararaj, U. Big returns from small fibers: A review of polymer/carbon nanotube composites. *Polym. Compos.* **2004**, *25*, 630–645.
18. Coleman, J.N.; Khan, U.; Blau, W.J.; Gun'ko, Y.K. Small, but strong: A review of the mechanical properties of carbon nanotube-polymer composites. *Carbon* **2006**, *44*, 1624–1652.
19. Wang, T.; Lei, C.H.; Liu, D.; Manea, M.; Asua, J.M.; Creton, C.; Dalton, A.B.; Keddie, J.L. A molecular mechanism for toughening and strengthening waterborne nanocomposites. *Adv. Mater.* **2008**, *20*, 90–94.
20. Wang, T.; Keddie, J.L. Design and fabrication of colloidal polymer nanocomposites. *Adv. Colloid Interf. Sci.* **2009**, *147–148*, 319–332.
21. Joussein, E.; Petit, S.; Churchman, J.; Theng, B.; Righi, D.; Delvaux, B. Halloysite clay minerals—A review. *Clay Minerals* **2005**, *40*, 383–426.
22. Lvov, Y.; Price, R. Halloysite Nanotubes in Nanomaterials Research. Available online: http://www.sigmaaldrich.com/materials-science/nanomaterials/nanoclay-building/halloysitenanotubes.html (accessed on 5 July 2011).
23. Qiao, J.Q.; Adams, J.; Johannsmann, D. Addition of Halloysite Nanotubes Prevents Cracking in Drying Latex Films. *Langmuir* **2012**, *28*, 8674–8680.

24. Rawtani, D.; Agrawal, Y.K. Multifarious Applications of Halloysite Nanotubes: A Review. *Rev. Adv. Mater. Sci.* **2012**, *30*, 282–295.
25. Shchukin, D.G.; Lamaka, S.V.; Yasakau, K.A.; Zheludkevich, M.L.; Ferreira, M.G.S.; Mohwald, H. Active anticorrosion coatings with halloysite nanocontainers. *J. Phys. Chem. C* **2008**, *112*, 958–964.
26. Machado, G.S.; Castro, K.; Wypych, F.; Nakagaki, S. Immobilization of metalloporphyrins into nanotubes of natural halloysite toward selective catalysts for oxidation reactions. *J. Mol. Catal. A Chem.* **2008**, *283*, 99–107.
27. Cho, S.H.; White, S.R.; Braun, P.V. Self-Healing Polymer Coatings. *Adv. Mater.* **2009**, *21*, 645–649.
28. Levis, S.R.; Deasy, P.B. Characterisation of halloysite for use as a microtubular drug delivery system. *Int. J. Pharm.* **2002**, *243*, 125–134.
29. Rooj, S.; Das, A.; Heinrich, G. Tube-like natural halloysite/fluoroelastomer nanocomposites with simultaneous enhanced mechanical, dynamic mechanical and thermal properties. *Eur. Polym. J.* **2011**, *47*, 1746–1755.
30. Barrientos-Ramirez, S.; de Oca-Ramirez, G.M.; Ramos-Fernandez, E.V.; Sepulveda-Escribano, A.; Pastor-Blas, M.M.; Gonzalez-Montiel, A. Surface modification of natural halloysite clay nanotubes with aminosilanes. Application as catalyst supports in the atom transfer radical polymerization of methyl methacrylate. *Appl. Catal. A Gen.* **2011**, *406*, 22–33.
31. Yuan, P.; Southon, P.D.; Liu, Z.W.; Green, M.E.R.; Hook, J.M.; Antill, S.J.; Kepert, C.J. Functionalization of halloysite clay nanotubes by grafting with gamma-aminopropyltriethoxysilane. *J. Phys. Chem. C* **2008**, *112*, 15742–15751.
32. Datasheet Bayhydrol® A XP 2695. Available online: http://www.bayercoatings.de/BMS/DBRSC/BMS_RSC_CAS.nsf/files/_Industrie/$file/Industrie_Primer_SA_Bayhydrol_A_XP_2695%20d.pdf (accessed on 23 August 2012).
33. Desmodur® N 3900. Available online: http://tecci.bayer.de/coatings/emea/de/Desmodur_N_3900_de.pdf?para=bd4ec657b1e201a9dca7a9f0a8bce840 (accessed on 5 September 2012).
34. Otts, D.B.; Cueva-Parra, L.A.; Pandey, R.B.; Urban, M.W. Film formation from aqueous polyurethane dispersions of reactive hydrophobic and hydrophilic components; Spectroscopic studies and Monte Carlo simulations. *Langmuir* **2005**, *21*, 4034–4042.
35. Hesse, M.; Meier, H.; Zeeh, B. *Spektroskopische Methoden in der Organischen Chemie*, 5 ed.; Georg Thieme Verlag: Stuttgart, Germany, 1995.
36. Foygel, M.; Morris, R.D.; Anez, D.; French, S.; Sobolev, V.L. Theoretical and computational studies of carbon nanotube composites and suspensions: Electrical and thermal conductivity. *Phys. Rev. B* **2005**, *71*, 104201.
37. Howarter, J.A.; Youngblood, J.P. Self-cleaning and next generation anti-fog surfaces and coatings. *Macromol. Rapid Commun.* **2008**, *29*, 455–466.